11

The global carbon cycle: interactions between the atmosphere and ocean

11.1 The global carbon cycle *page* 373
11.2 The biological and solubility pumps of the ocean 376
11.2.1 The solubility pump 379
11.2.2 The biological pump 381
11.3 The fate of anthropogenic CO_2 in the ocean 384
11.3.1 The carbonate buffer factor (Revelle factor) 386
11.3.2 Methods of measuring anthropogenic CO_2 uptake 393
11.3.3 Partitioning anthropogenic CO_2 among the ocean, atmosphere, and terrestrial reservoirs 398
References 402

Cycling of carbon among the ocean, atmosphere and land is a fundamental component of the chemical perspective of oceanography because the fugacity (f_{CO_2}) or partial pressure (p_{CO_2}) of carbon dioxide is the most important greenhouse gas in the atmosphere (except for H_2O, which behaves in a feedback rather than forcing capacity). Since there is about 50 times as much inorganic carbon dissolved in the sea as there is CO_2 in the atmosphere, ocean carbonate chemistry has a great impact on f_{CO_2} in the atmosphere. On time scales of hundreds to a thousand years the main marine processes that influence f_{CO_2} in the atmosphere are the thermodynamic temperature dependence of CO_2 solubility in seawater (the *solubility pump*), and the interplay between the rate of ocean circulation and the rate of biological carbon removal from the euphotic zone to the deeper reservoirs of the ocean (the *biological pump*). On longer time scales, of the order of one to tens of thousands of years, the preservation and dissolution of calcium carbonate along with the rate of weathering and the transport of bicarbonate to the sea come more into play.

The Earth is presently in the early stages of a grand acid–base titration of seawater by CO_2. Anthropogenic CO_2 is being added to the atmosphere at a rate fast enough to have resulted in an approximately 30% increase in the f_{CO_2} of the atmosphere since pre-industrial time. Only about 40% of the CO_2 added to the atmosphere has

//FS2/CUP/3-PAGINATION/ERN/2-PROOFS/3B2/9780521833134C11.3D 373 [372–403] 29.1.2008 12:58PM

remained there: the rest has gone into the land and ocean carbon reservoirs. It is extremely important that we understand the processes controlling the uptake of CO_2 because future prediction of global climate will depend on knowing how CO_2 partitions between the atmosphere, land, and ocean.

The long-term response of the ocean's carbonate system to past climate perturbations, on time scales ranging from ten thousand to hundreds of millions of years, involves the interaction of the seawater carbonate system with the carbonate solids deposited in marine sediments. For example, there are very large changes in the calcium carbonate content of deep-sea sediment cores that span past glacial–interglacial times from all the ocean basins that tell us something about past excursions in the chemistry of the sea and atmosphere. Interpreting these records requires an understanding of the present-day relation between carbonate chemistry and $CaCO_3$ preservation in marine sediments.

In this chapter we explain the most important processes controlling the interaction of carbon between the atmosphere and ocean. Processes affecting $CaCO_3$ burial are reviewed in the following chapter on sediment diagenesis. We begin this chapter with an overview of the global carbon cycle, then describe the role of steady-state processes involving the ocean's solubility and biological pump, and end with a discussion of the fate of CO_2 from anthropogenic perturbation.

11.1 The global carbon cycle

The global carbon cycle involves reactions within and exchange among the major global reservoirs: atmosphere, ocean and land (Fig. 11.1). The important reactions are formation and destruction of organic matter and calcium carbonate via photosynthesis/respiration and precipitation/dissolution, respectively. Exchange among the reservoirs is primarily via CO_2 gas exchange, flow of dissolved inorganic carbon ($DIC = HCO_3^- + CO_3^{2-} + CO_2$) in rivers, and the burial of the mineral $CaCO_3$.

The amount of carbon in each of the main global reservoirs and the exchange fluxes (Table 11.1, Fig. 11.1) provides a qualitative impression of how much the reservoirs depend on one another. Among the atmosphere, land and ocean the carbon reservoir size of the atmosphere is by far the smallest (600 Pg before anthropogenic changes, where $1\,Pg = 10^{15}$ g); DIC of the ocean the largest (38 000 Pg) and the exchangeable reservoirs in land plants and soils are somewhere in between (*c.*2000 Pg). Since atmosphere–land and atmosphere–ocean CO_2 exchange rates are about the same (on the order of 100 Pg y^{-1}), it is pretty clear that the pressure of CO_2 in the atmosphere is a slave to processes that occur in the larger reservoirs.

There are two categories of flux depicted in Fig. 11.1: "long-term" fluxes, indicated by dashed arrows, and "short-term" fluxes, indicated by solid arrows. The "long-term" fluxes represent fluxes

//FS2/CUP/3-PAGINATION/ERN/2-PROOFS/3B2/9780521833134C11.3D 374 [372–403] 29.1.2008 12:58PM

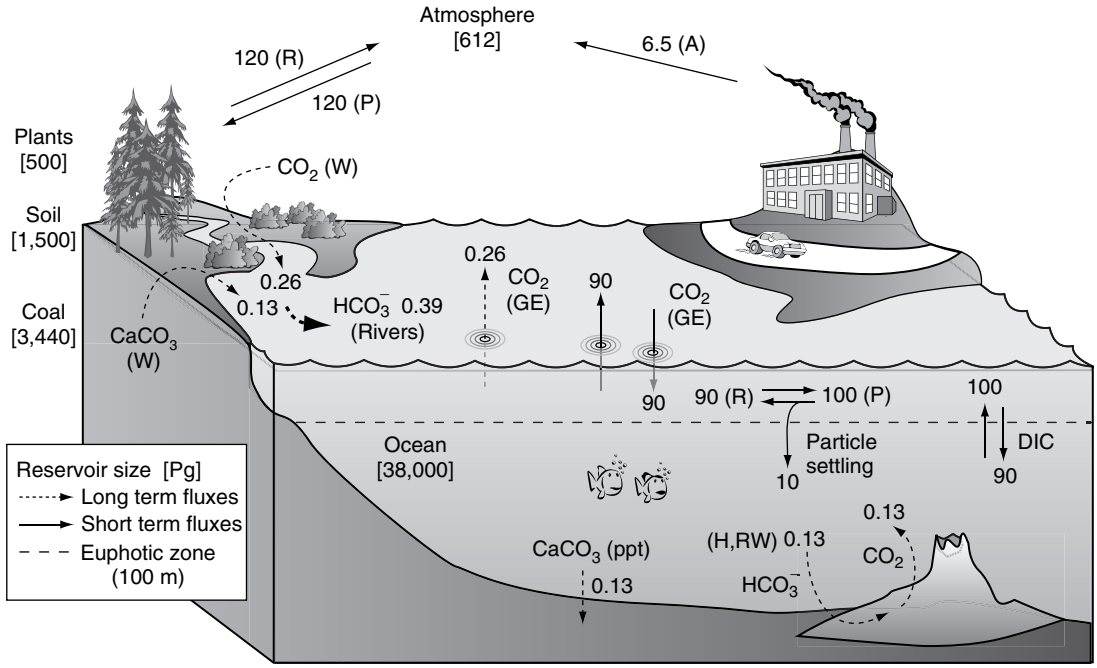

Figure 11.1. The global carbon cycle. Values in brackets are preanthropogenic reservoir sizes in Pg (10^{15} g); values on the arrows are fluxes in Pg y^{-1}. Dashed lines represent the long-term carbon cycle determined by weathering. Values are normalized to the flux of DIC from rivers (see Chapter 2). Solid arrows are the shorter-term carbon fluxes associated with photosynthesis and respiration. The wiggly vertical line indicates particulate C and DOC transport from the ocean euphotic zone to deep water. Symbols: W, weathering of carbonates ($CaCO_3 + CO_2 + H_2O \rightarrow 2HCO_3^- + Ca^{2+}$) and silicates (silicate $+ CO_2 + H_2O \rightarrow$ clay $+ HCO_3^-$ + cations); GE, gas exchange; P, gross photosynthesis ($CO_2 + H_2O \rightarrow CH_2O$ (OM) $+ O_2$); R, respiration (CH_2O (OM) $+ O_2 \rightarrow CO_2 + H_2O$); pptn, calcite precipitation (the reverse of carbonate weathering); H, hydrothermal processes; RW, reverse weathering (the reverse of silicate weathering).

associated with processes of weathering; the "short-term" fluxes are those that are driven primarily by photosynthesis and respiration. Each of these mechanisms controls the f_{CO_2} in the atmosphere on different time scales. Changes in weathering reactions due to sea-floor spreading and tectonics such as mountain building are believed to have been the major factors for regulating the CO_2 content of the atmosphere through the early history of the Earth on 10–100 million year time scales (see, for example, Berner, 1990). More recent fluctuations of f_{CO_2} on glacial–interglacial time scales (10–100 000 years) observed in trapped atmospheric bubbles in ice cores were probably influenced by the shorter-term fluxes involving ocean circulation and biological processes in the ocean and on land (see Chapter 7).

The present-day weathering fluxes depicted in Fig. 11.1 are normalized to the flux of DIC (primarily HCO_3^-) that enters the ocean via the world's rivers (*c*.0.4 Pg y^{-1}) (Table 2.3). Since we know that the ultimate origin of weathering-produced carbon is from the atmosphere and $CaCO_3$ rocks on an approximately 2:1 basis (see Fig. 2.2), all other fluxes can be scaled accordingly. The flux of CO_2 out of the atmosphere (0.26 Pg y^{-1}), that provides the acid for dissolution of rocks in soils via weathering and flows to the ocean as HCO_3^-, must be matched by an equal return flux to the atmosphere. This return flux derives partly from precipitation of $CaCO_3$ in the ocean (reaction (iii) in Table 2.2, also given in the caption to Fig. 11.1), which is supported by the Ca^{2+} and HCO_3^- flow from rivers. The other contribution to the return of CO_2 to the atmosphere is via a reaction to form silicate rocks that is the equivalent of reverse weathering (the reverse of reaction (vi) in Table 2.2, also reproduced in the caption to Fig. 11.1) and occurs either in ocean sediments or at hydrothermal areas. Even

//FS2/CUP/3-PAGINATION/ERN/2-PROOFS/3B2/9780521833134C11.3D 375 [372–403] 29.1.2008 12:58PM

Table 11.1. *Carbon reservoirs (excluding terrestrial rocks other than coal) and fluxes*

Reservoirs (Pg)			
Atmosphere: CO_2 (288 ppm in 1850)			612
	(369 ppm in 2000)		784
Oceans:	Biota		1–2
	DOC		700
	Org. C in sediments (1 m)		1000
	DIC		38 000
Terrestrial:	Biota		600
	Soil humus (1 m)		1500
	Fossil fuels (identified reserves):	gas	44
		oil	90
		coal, oil sand and shale	3440
Fluxes (Pg y^{-1})			
Atmosphere–ocean exchange			90
Gross primary production: ocean			100
land			120
Net primary production: ocean			45
land			60
Net C export from the surface ocean			8–15
Sedimentation of org. C in the ocean			0.2
Anthropogenic changes (Pg or Pg y^{-1})			
Cumulative changes (Pg) (1800–1994)			
Fossil fuels burnt and cement produced			244
Atmospheric increase			165
Storage in the ocean			118
Inferred terrestrial change			−39
Partitioning of anthropogenic fluxes (1990s) (Pg y^{-1})			
Fossil fuel and cement production			6.3 ± 0.4
Atmosphere accumulation			3.2 ± 0.1
Uptake by terrestrial biosphere			-1.4 ± 0.7
Ocean uptake			-1.7 ± 0.5

Source: The data are from the compilations of Pilson (1998), IPCC (2001), and Sabine *et al*. (2004).

though these fluxes are much smaller than those involved in the "short-term" CO_2 exchange, they are known at least as well because they are constrained by the chemical concentrations and flow of rivers.

The larger "short-term" fluxes are mainly controlled by the processes of photosynthesis and respiration. In the case of the atmosphere–land exchange CO_2 is taken up directly from the atmosphere by photosynthesis in leaves and released from the plants and soils to the atmosphere via respiration. The uptake and release are balanced (except for the 0.26 Pg of CO_2 that ultimately goes to weathering rocks in the soil) as long as the plant and soil reservoirs are not changing. The exchange of CO_2 between the atmosphere and ocean represents the one-way gas exchange flux and is controlled by the f_{CO_2}

//FS2/CUP/3-PAGINATION/ERN/2-PROOFS/3B2/9780521833134C11.3D 376 [372–403] 29.1.2008 12:58PM

and the gas exchange mass transfer coefficient (see Chapter 10). In pre-industrial times the mean f_{CO_2} of the atmosphere and ocean were about the same, so the one-way fluxes across the air–water interface were also about the same (*c.*90 Pg y^{-1}). It is fortuitous that the atmosphere–ocean exchange rate of CO_2 is about equal to marine euphotic zone gross photosynthesis and respiration rates (*c.*100 Pg y^{-1}).

Categorization of carbon fluxes in the ocean (Fig. 11.1) is more detailed than on land because rates of gas exchange and biological processes can be separated. The difference between organic carbon production by photosynthesis and respiration in the marine euphotic zone is about 10% of the rate of photosynthesis and equal to the transport of organic carbon to the ocean interior by sinking particulate material and mixing of dissolved organic carbon (DOC). This is the marine "biological carbon pump." A similar process occurs on land between the living biomass and humic material, but it is more heterogeneous and difficult to characterize. Although the marine biological carbon pump is only about one tenth of the photosynthesis in the ocean, it represents a relatively large flux (*c.*10 Pg y^{-1}) away from contact with the atmosphere into the long-term deep-ocean DIC reservoir. The analogous reservoir on land is soil carbon, which is about 30 times smaller and has a shorter residence time. Thus, changes in the magnitude of the ocean's biological pump may have had a large influence on the f_{CO_2} of the atmosphere in the past and could also be important in controlling future f_{CO_2}.

Fluxes and reservoirs in Fig. 11.1 are those believed to be representative of pre-industrial values. Comparison of these values with the rate of input of CO_2 to the atmosphere via fossil fuel burning and cement production (*c.*6.2 Pg y^{-1}) places the anthropogenic input into perspective with natural processes. The anthropogenic perturbation is about 20 times smaller than the one-way exchange of CO_2 between the atmosphere and ocean and the rates of photosynthesis on land or in the ocean, but about 20 times larger than the fluxes of CO_2 from global weathering and about half the present biological carbon pump to the deep ocean. This perturbation is by all measures very large compared with natural fluxes. The amount of fossil fuel that has been burnt since 1800 (*c.*244 Pg) (Table 11.1), is greater than the known reserves of gas and oil but less than *c.*10% of the known coal reserves. Coal reserves, albeit very large, are still only about one tenth the size of the ocean's DIC reservoir. In the following sections we demonstrate in a simple quantitative way the influence of steady-state processes on the f_{CO_2} of the atmosphere and review what is known about the fate of carbon anthropogenically introduced into the atmosphere.

11.2 The biological and solubility pumps of the ocean

The carbon pump in the ocean refers to processes that create a vertical gradient in the dissolved inorganic carbon (DIC) concentration. These

//FS2/CUP/3-PAGINATION/ERN/2-PROOFS/3B2/9780521833134C11.3D 377 [372–403] 29.1.2008 12:58PM

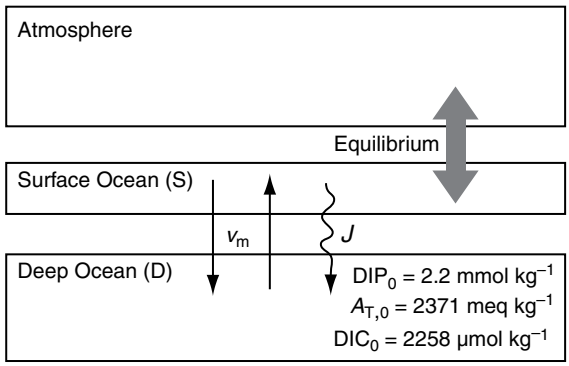

Figure 11.2. Sketch of the three-box model of the atmosphere, surface and deep ocean. Equations indicate the circulation dynamics (V_m in m y^{-1}, is the mixing rate between the surface and deep ocean); stoichiometry of the particulate transport (J in mol m^{-2} y^{-1}); and chemical equilibria of the carbonate system.

$$\text{Dynamics: } V_D \times \frac{d[C_D]}{dt} = 0 = V_m \times ([C_S] - [C_D]) + J$$

$$\text{Stoichiometry: } \Delta P : \Delta N : \Delta DIC : \Delta A_T : \Delta Ca$$
$$1 : 16 : 136 : 44 : 30$$

Equilibrium:

$$DIC = [HCO_3^-] + [CO_3^{2-}] + [CO_2]$$

$$A_{C\&B} = [HCO_3^-] + 2 \times [CO_3^{2-}] + [B(OH)_4^-]$$

$$B_T = B(OH)_3 + B(OH_4^-)$$

$$K_{H,CO_2} = \frac{[CO_2]}{f^a_{CO_2}} \qquad K'_2 = \frac{[CO_3^{2-}][H^+]}{[HCO_3^-]}$$

$$K'_1 = \frac{[HCO_3^-][H^+]}{[CO_2]} \qquad K'_B = \frac{[B(OH)_4^-][H^+]}{[B(OH)_3]}$$

processes move DIC from the upper *c.*100 m of the ocean to the ocean's interior and thus decrease the amount of carbon in the surface ocean and atmosphere. This carbon transfer has been categorized into the "solubility" and "biological" carbon pumps (Volk and Hoffert, 1985). The strength of the solubility pump is measured by the gradient in temperature between the surface and deep ocean. Dense colder water can hold more DIC at thermodynamic equilibrium with atmospheric f_{CO_2} so this process increases the DIC content of deeper waters. The strength of the biological pump is determined by the vertical gradient of nutrients created by the transport of organic matter in the form of particles and dissolved organic matter (DOM) from the euphotic zone to deeper waters. The stoichiometric relation between nutrient and DIC uptake and regeneration during biological processes then determines the biologically produced vertical gradient of DIC in the ocean.

A very simple demonstration of the importance of ocean temperature, marine biology and ocean dynamics to atmospheric f_{CO_2} is achieved by using a three-box model (Fig. 11.2) of the ocean and atmosphere that is similar to the two-layer model introduced in Chapter 6. This construct can be used to show the sensitivity of atmospheric f_{CO_2} to ocean surface temperature, biological processes

//FS2/CUP/3-PAGINATION/ERN/2-PROOFS/3B2/9780521833134C11.3D 378 [372–403] 29.1.2008 12:58PM

and overturning circulation. In this calculation we concern ourselves only with steady-state natural concentrations that are uninfluenced by human activities. Although this model involves gross approximations, it is a jewel in demonstrating the mechanisms that are necessary for the implementation of these concepts in more complicated models with more boxes (see, for example, Toggweiler, 1999) and global circulation models (see, for example, Archer *et al.*, 2000).

In this simple three-box model one assumes the entire atmosphere, surface and deep ocean each have homogeneous concentrations. The well-mixed approximation for the atmosphere is not bad, as measurements of f_{CO_2} indicate that differences from place to place are only a few percent. The north–south hemispheric gradient is only 1%–2%, and this is primarily caused by greater fossil fuel usage in the north. The homogeneous surface and deep ocean assumptions, however, are extreme approximations because of the vast differences in global temperature and biological productivity. We use averages, which undoubtedly lead to results that are only crudely accurate.

It is assumed in this calculation that the atmosphere and surface ocean are in chemical equilibrium with respect to carbon. That is, the f_{CO_2} of the atmosphere equals the f_{CO_2} in the surface ocean. Although this is not the case in many areas, ocean surveys indicate that atmospheric f_{CO_2} is on average about 8 ppm higher than that of the surface ocean, or only 2% greater in the atmosphere. Again, most of the atmosphere excess is caused by anthropogenic fossil fuel burning: the pre-industrial mean surface ocean and atmosphere f_{CO_2} values were probably nearly equal.

Since we assume the atmosphere and ocean are in chemical equilibrium, and the input from rivers and burial in the sediments are small compared to the other fluxes, the entire dynamics of the model is reduced to the rate of surface–deep mixing and the sinking of particles. (For simplicity, DOC transport is not considered in this simple model.) One can see that for a steady state to be achieved the flux of carbon to the surface ocean must equal the sinking flux of particles. The mean residence time for deep water is that determined by natural ^{14}C measurements (see Chapter 6): 500–1000 y.

The chemical currency of the ocean model consists of three dissolved constituents: DIC and alkalinity for carbon, and phosphate for nutrients. DIC and alkalinity are used to represent the carbon system because they are total carbon and charge quantities that are independent of temperature and pressure (i.e. they do not vary in concentration because of temperature differences between surface and deep waters as do their constituents, HCO_3^-, CO_3^{2-} and CO_2). There is also a thermodynamic temperature dependence between these chemical parameters and f_{CO_2}, and they change in clearly defined ways relative to nutrients during biological transformations. Dissolved inorganic phosphate (we use the symbol DIP here, but it is often represented as simply PO_4^{3-}) represents nutrients in the model. We could also have chosen nitrate (NO_3^-); however, we avoid the complications of nitrogen fixation and denitrification by choosing phosphate, and

//FS2/CUP/3-PAGINATION/ERN/2-PROOFS/3B2/9780521833134C11.3D 379 [372–403] 29.1.2008 12:58PM

biological uptake and release of both nutrients are related by a constant ratio (Fig. 6.2). Micronutrients like iron are not considered in this very simplified model. The deep concentrations of alkalinity, DIC and DIP are the mean values for the world's ocean: 2371 eq kg^{-1}, 2258 mol kg^{-1} and 2.2 mol kg^{-1}, respectively.

Model geometry and parameters are compiled in Fig. 11.2. The strategy is to determine the concentrations of alkalinity and DIC in the surface ocean layer from the equations that describe the model dynamics and the deep ocean values, and then to calculate the f_{CO_2} in thermodynamic equilibrium with these values at the mean surface water temperature and salinity. Carbonate plus borate alkalinity, $A_{C\&B}$, will be employed in our carbonate equilibrium calculations. (See Chapter 6 for a discussion of the carbonate equilibrium calculations.)

The change in concentration of a dissolved constituent, [C], in the deep reservoir is:

$$V_D \frac{d[C]}{dt} = 0 = v_m \left([C]_S - [C]_D \right) + J_C \tag{11.1}$$

where v_D is the deep reservoir volume, v_m is the mixing rate ($m^3\ y^{-1}$), $[C]_S$ and $[C]_D$ are the surface and deep concentrations, respectively (mol m^{-3}) and J_C is the biological flux to the deep reservoir in units of mol y^{-1}. Because this is a steady-state calculation we assume the left side of Eq. (11.1) is equal to zero. To a good first approximation, the only concentration variable is $[C]_S$ because the volume of the deep ocean is so much greater than the surface that the deep concentration cannot change appreciably from the total average values. One can write three equations of this type for DIP, DIC and $A_{C\&B}$. These equations are related through the biological flux terms, J_C, and the stoichiometric ratios, r, described later in the Section 11.2.2.

11.2.1 The solubility pump

The results of calculations to determine the sensitivity of atmospheric f_{CO_2} to changes of the solubility and biological pumps are presented in Table 11.2. An accurate model estimate of change requires a much more elaborate resolution of surface temperature, nutrient concentration and circulation than is possible with this crude model, but the basic principles and trends can be demonstrated. The *standard case* is determined by using a weighted mean surface temperature of 20 °C. This is a crude estimate, as equatorial mean values are 27 °C, subtropical values are on annual average 23 °C and high-latitude annual mean values are <10 °C. The surface-water phosphate value also represents a weighted mean between near zero values in subtropical surface waters and higher values in the Equator and high latitudes. The $[DIP]_S$ value of 0.5 mol kg^{-1} is chosen to generate an f_{CO_2} value that is near that measured in the atmosphere by using the calculation procedures described in the next section.

Changes in f_{CO_2} brought about by solubility are caused by the temperature dependence of the equilibrium constants. The model

//FS2/CUP/3-PAGINATION/ERN/2-PROOFS/3B2/9780521833134C11.3D 380 [372–403] 29.1.2008 12:58PM

Table 11.2. *The effect of the solubility and biological pumps on the fugacity of CO_2 in the atmosphere, f_{CO_2}, determined by the simple two-layer ocean model depicted in Fig. 11.2*

The first row is the standard case and the rows under this indicate changes due to temperature, carbon flux, circulation rate and the organic carbon to $CaCO_3$ ratio of the particle flux, OC : $CaCO_3$.

	Temp	$[DIP]_S$	τ_{mix}	$R_{OC:CA}$	DIC_S	$A_{T,S}$	f_{CO_2}
Case	°C	μmol kg^{-1}	y		μmol kg^{-1}	μeq kg^{-1}	atm
Standard	20	0.5	1000	3.5	2027	2296	375
Temp. effect	15						304
	25						460
Biol. pump							
Carbon flux	20	2.2			2258	2371	1184
		0.0			1959	2274	293
Circulation		0.85	500		2074	2312	446
		0.0	1500		1959	2274	291
OC:$CaCO_3$ (P:OC = 106)		0.5	1000	10:1	2059	2361	337
				1.5:1	1957	2157	485

results indicate that atmospheric f_{CO_2} in equilibrium with seawater decreases when the temperature of the water is colder. Although the temperature response of CO_2 depends on all three carbonate equilibrium constants, K_H, K_1' and K_2', and the borate equilibrium constant, K_B, (Chapter 4) the combined temperature dependence of CO_2 solubility trends in the same direction as that for unreactive gases: colder water can accommodate more CO_2. Atmospheric f_{CO_2} changes by about 15 μatm per degree change in surface water temperature. This result suggests that global warming has a positive feedback: higher temperatures will expel more CO_2 from the ocean. Decreases in global temperature during the last ice age would tend to draw down atmospheric f_{CO_2} as more would have been dissolved in the ocean. This is in the direction observed for f_{CO_2} changes during glacial periods (Chapter 7), but the change in our simple model is about twice that of more realistic global models. It has been shown in many different more realistic models that a reduction in global ocean surface temperatures of 3–5 degrees (coupled with an increase in salinity due to the change in global ice volume) can account for a decrease in atmospheric f_{CO_2} of between 20 and 30 ppm out of a measured decrease of about 80 ppm (Sigman and Boyle, 2000).

Probably the most important dynamic of the solubility pump that the simple model in Fig. 11.2 misses is a large horizontal temperature gradient in the surface ocean. Water upwelled at the Equator is heated and degasses to the atmosphere as it flows north and south. At high latitudes the same water is cooled to the point where it reabsorbs some of the CO_2 it lost to the atmosphere before it downwells to the ocean interior. Thus, any change in the f_{CO_2} of the

//FS2/CUP/3-PAGINATION/ERN/2-PROOFS/3B2/9780521833134C11.3D 381 [372–403] 29.1.2008 12:58PM

atmosphere resulting from global temperature changes and the consequent effect on the solubility pump would also depend on the latitudinal distribution of the temperature change. In spite of this weakness the sense of the relative changes to expect in the solubility pump are clear from the simple model.

11.2.2 The biological pump

Modern studies of the biological pump began with investigations of the mechanism of surface to deep carbon transfer used in box models (e.g. Broecker, 1971) together with the conceptual link between the experimental investigations of particle fluxes and biological production (Eppley and Peterson, 1979). These studies approached the problem from the points of view of both biological and chemical oceanography and have become in recent years prime examples of interdisciplinary oceanographic investigations.

In order to determine the sensitivity of atmospheric f_{CO_2} to the flux of biological particles, J, in Fig. 11.2, one must establish the chemical content of the sinking material. More precisely, one needs to know how the degradation and dissolution of the particulate matter changes the water chemistry of the deep ocean. In the discussions of life in the ocean (Chapter 6) we established that the Redfield ratios for changes in P, N, and C during organic matter production and degradation are close to their traditional values:

$$\Delta P : \Delta N : \Delta C_{organic} = 1 : 16 : 106. \tag{11.2}$$

For every mole of DIP added to the water by organic matter degradation, 106 moles of C (as DIC) are added. The oxidation of NH_3 to NO_3^- generates a proton and thus decreases alkalinity by one equivalent for each of the 16 moles of NH_3 oxidized per mol of PO_4 added during organic matter degradation. This creates a stoichiometry for change in deep-water DIC and alkalinity with respect to phosphorus by organic matter degradation of:

$$\Delta P : \Delta N : \Delta DIC : \Delta A_{C\&B} = 1 : 16 : 106 : -16. \tag{11.3}$$

Calcium carbonate is the only other constituent of biologically produced matter other than organic carbon and nitrogen that creates a substantial change in the DIC and alkalinity of seawater. Observed alkalinity : DIC ratio changes in the ocean below the euphotic zone require degradation of organic carbon and dissolution of $CaCO_3$ in a ratio of about 10 to explain the surface to deep Atlantic changes and between 1 and 2 to explain the trends following the deep ocean circulation (between 2–4 km depth) (Fig. 4.6). For the purposes of a two-layer ocean one needs a composite value for the ocean below 100 m, which skews the average OC : $CaCO_3$ ratio in sinking particulate material toward those below the thermocline, and the ratio for this model becomes 3.5 : 1. Thus, one mole of $CaCO_3$ is produced or dissolves for every 3.5 moles of organic matter produced or degraded. The DIC change attributed to $CaCO_3$ for one mole of phosphorus

//FS2/CUP/3-PAGINATION/ERN/2-PROOFS/3B2/9780521833134C11.3D 382 [372–403] 29.1.2008 12:58PM

change is 106/3.5 = 30. Since production or dissolution of $CaCO_3$ creates a 2 : 1 change in Alk : DIC, the composite stoichiometric change for the modern ocean in our model becomes:

$$\Delta P : \Delta N : \Delta DIC : \Delta A_{C\&B} = 1 : 16 : 136 : 44. \tag{11.4}$$

To determine the surface ocean concentration of DIC and $A_{C\&B}$ as a function of surface–deep gradient of DIP, one can write three steady-state versions of Eq. (11.1) for DIP, DIC and $A_{C\&B}$. These equations are related through the biological flux terms J_C, and the stoichiometric ratios, r, given in equations like that in (11.4):

$$J_{DIC} = J_P\, r_{DIC:P}\ ;\ J_A = J_P\, r_{A:P}. \tag{11.5}$$

By combining the phosphorus equation with those for alkalinity and DIC, the ratio v_m/J_C can be eliminated to demonstrate the steady-state surface–deep water differences for DIP, DIC, and $A_{C\&B}$:

$$DIC_S - DIC_D = \left([DIP]_S - [DIP]_D \right) r_{DIC:P} \tag{11.6}$$

$$A_{C\&B,\,S} - A_{C\&B,\,D} = \left([DIP]_S - [DIP]_D \right) r_{A_T:P}. \tag{11.7}$$

Assuming that the mean deep-water concentrations are constants because this reservoir is so large compared with the surface layer, one can determine the surface-water values of DIC and $A_{C\&B}$ as a function of the surface–deep differences in DIP. When this is done the carbonate equilibrium equations (Chapter 4, Fig. 11.2) can be used to determine f_{CO_2}.

The response of our simple ocean and atmosphere model to changes in the biological pump (Table 11.2) is manifested in three ways. The best indicator of the effect of the biological pump is the concentration difference in phosphate between the surface and deep ocean. Because of Eq. (11.1), any change in the ratio of the particle export to surface–deep mixing, v_m/J_C, must be accompanied by a change in the surface–deep differences. In response to an increase in particle flux or a decrease in circulation the gradient in limiting nutrient concentration between the surface and deep ocean must increase. The biological pump (particle flux) change scenarios in Table 11.2 represent the most extreme cases in surface ocean nutrient concentrations in which the DIP concentration in surface waters is either equal to the deep value or zero. The former case is the "Strangelove Ocean" in which there is no biological pump at all. This is the chemical equilibrium ocean. Something like this may have happened at the time of the last mass extinctions in geologic history. Sixty million years ago at the Cretaceous–Tertiary boundary it is believed that a meteor collided with the Earth and 80% of existing species became extinct. Without the biological carbon pump, the model predicts that the atmosphere would have an f_{CO_2} of about 1000 atm. The actual value may not be accurate because of the simple model architecture, but the trend toward increasing f_{CO_2} is clear. In the other extreme, when the nutrients in surface waters are entirely

//FS2/CUP/3-PAGINATION/ERN/2-PROOFS/3B2/9780521833134C11.3D 383 [372–403] 29.1.2008 12:58PM

depleted, the maximum effect of the biological pump is realized. In our three-box model this causes an 80 ppm decrease from the standard case. Given this large effect, one can readily understand why marine scientists and paleoclimatologists have focused on the change in efficiency of high-latitude nutrient utilization in surface waters as a means for explaining past changes in atmospheric f_{CO_2} (see Chapter 7).

If the particle export remains unchanged but the mixing rate is altered, the DIP gradient between surface and deep waters changes. This is demonstrated in the biological pump (circulation) section of Table 11.2 by varying the residence time of the water in the deep ocean between 500 and 1500 y. If the residence time becomes smaller (i.e. circulation faster), the gradient from surface to deep concentrations becomes smaller and atmospheric f_{CO_2} increases, creeping in the direction of the chemical equilibrium ocean. The opposite is true if circulation decreases. In this case atmospheric f_{CO_2} drops until all the nutrients are consumed in the surface waters and then the surface–deep gradient can increase no more. When surface nutrients are totally depleted, any decrease in mixing must be matched exactly by a decrease in J_C to maintain a constant v_m/J_C ratio.

As long as the nutrient concentration in surface waters is greater than zero the biological term, J_C, and the mixing term, v_m, are independent: changes in either term can cause a change in the atmospheric f_{CO_2}. This case is analogous to today's ocean at high latitudes, where productivity and the biological pump are limited by factors other than the flux of nutrients from the deep ocean to surface waters. Surface nutrient concentrations are high in these regions because the probability of their removal by biological production is of the same magnitude as exchange with deeper waters by mixing. As long as our simple two-layer model has finite nutrient concentration in the surface ocean, its response is most analogous to today's high-latitude ocean. On the other hand, when nutrient concentrations in the surface ocean are totally depleted so that the biological pump is limited by the flux of nutrients from deep waters to the surface ocean, there is no atmospheric response to circulation changes. The reason for this insensitivity is that when surface nutrients are totally depleted, the surface ocean–deep ocean nutrient gradient is constant, so a change in the nutrient flux to the surface must be exactly compensated by changes in the particle export rate (see Eq. (11.1)). This might be similar to the situation in the subtropical oceans today, where nutrient concentrations in surface waters are very low.

The dependence of f_{CO_2} on the chemical character of the biological debris that is produced in the surface ocean is demonstrated in the model by the last sensitivity analysis in Table 11.2 (biological pump – OC : $CaCO_3$). If the organic carbon to $CaCO_3$ ratio of the particulate material, $r_{OC:Ca}$, becomes greater than in the standard case (poorer in $CaCO_3$) while maintaining the same phosphate : organic matter ratio, there will be less alkalinity removed from surface waters per mole of DIC removed. Since the $A_{C\&B}$: DIC ratio in surface waters is about equal to $[CO_3^{2-}]$ (see Chapter 4), this difference and the carbonate ion

//FS2/CUP/3-PAGINATION/ERN/2-PROOFS/3B2/9780521833134C11.3D 384 [372–403] 29.1.2008 12:58PM

concentration will become greater under this scenario. Higher CO_3^{2-} concentrations mean more basic waters and lower f_{CO_2} (Fig. 4.2). Changing the particulate carbon flux ratio $r_{OC:Ca}$ from 3.5 to 10 in the model decreases the atmospheric f_{CO_2} by about 40 μatm.

If the particulate matter carbonate : carbon ratio changed in the opposite sense to near unity (i.e. a much greater flux of $CaCO_3$ relative to organic matter), this would decrease the alkalinity of surface waters relative to DIC because the formation and removal of $CaCO_3$ decreases $A_{C\&B}$ and DIC in a ratio of 2 : 1. A greater decrease in $A_{C\&B}$ relative to DIC would make the $A_{C\&B}$ – DIC difference smaller, decreasing the surface water CO_3^{2-} concentration and increasing f_{CO_2}. In the model a decrease in the $r_{OC:Ca}$ ratio from 3.5 to 1.5 causes an increase in f_{CO_2} by 110 μatm.

Formation and removal of organic matter and $CaCO_3$ have opposite effects on the f_{CO_2} of the atmosphere. An organic carbon-rich flux from the euphotic zone decreases atmospheric CO_2, whereas a $CaCO_3$-rich flux increases it. Thus, the ratio of coccolithophorids ($CaCO_3$-secreting autotrophic plankton) to other non-$CaCO_3$-secreting organisms that grow in the ocean's surface waters has important consequences for the f_{CO_2} in the atmosphere. If surface waters become more hostile to $CaCO_3$-secreting organisms because of increases in anthropogenic CO_2, as some controlled experiments on the effects of lower marine surface-water pH suggest, and the organic carbon portion of the biological pump remains the same, the ocean will respond with a negative feedback, tending to lower the f_{CO_2} of the atmosphere by slowing down the carbonate-related portion of the biological pump. Paleoceanographers search deep-sea sediment cores for evidence of changes in the rates of burial of diatoms (opal shells) and coccolithophorids through geologic time because of their potential ramifications for past levels of atmospheric CO_2. However, relating the preservation of carbonate and opal shells to their rain rates from the euphotic zone has so far been achieved only qualitatively because a large portion of the tests of both these phytoplankton taxa dissolve before they are buried in marine sediments.

Results from the simple ocean–atmosphere model in Fig. 11.2 and Table 11.2 demonstrate the fascinating ramifications of changing sea-surface temperatures and the interplay between biological fluxes and ocean circulation for atmospheric f_{CO_2}. Present coupled atmosphere–ocean models suggest that a doubling of atmospheric f_{CO_2} would result in a 2–4 °C mean global temperature increase. Ocean circulation and sea-surface ecology are also sensitive to temperature and f_{CO_2} changes, which will provide feedbacks that oceanographers are striving to understand quantitatively.

11.3 The fate of anthropogenic CO_2 in the ocean

Great advances in our understanding of the fate of fossil fuel CO_2 began with two seminal studies: the onset of monitoring the f_{CO_2} of

//FS2/CUP/3-PAGINATION/ERN/2-PROOFS/3B2/9780521833134C11.3D 385 [372–403] 29.1.2008 12:58PM

the atmosphere by Dave Keeling, starting in 1958 (see, for example, Keeling, 1960) and studies of the CO_2 buffering capacity of the ocean (Revelle and Suess, 1957). These investigations demonstrated that only a portion of the CO_2 introduced to the atmosphere was accumulating there, and that the ocean's surface layer had limited potential to adsorb the rest. Subsequent descriptions of the dynamics of the process of CO_2 adsorption by the ocean by using a series of box and multi-layer models were forerunners for introducing chemistry into present-day global circulation models (GCMs).

Even though the magnitude of the flux controlled by the biological pump (10–15 Pg y^{-1}) is similar to the anthropogenic CO_2 flux to the atmosphere (*c.* 6 Pg y^{-1}), it is by no means clear that the latter has any effect on the former. Since the limiting factors for biological organic carbon export from the surface ocean are nutrients and light, there is not a direct effect of anthropogenic CO_2 contamination on the rate of biological processes. However, warming of the Earth caused by greenhouse gas increase may change the circulation of the ocean and atmosphere, and this could in turn affect the rate of nutrient delivery to the ocean's euphotic zone. The uncertainties in the processes involved are presently so great that we are not sure of the magnitude or even the direction of this potential effect. We shall assume here that the processes controlling anthropogenic CO_2 uptake in the ocean are physical and thermodynamic, and that there is no effect on the biological pump.

The atmospheric burden of anthropogenic CO_2 is very well known because it has been measured since 1958; and recent ice core studies indicate how the atmospheric CO_2 evolved between the pre-industrial period and 1958 (Fig. 11.3). Because industries and governments keep records of the amount of fossil fuel recovered, this number is also known. The amount of atmospheric CO_2 increase over the period 1860–1989 is estimated to be only 40% of total emissions (Table 11.1). Where has the rest gone?

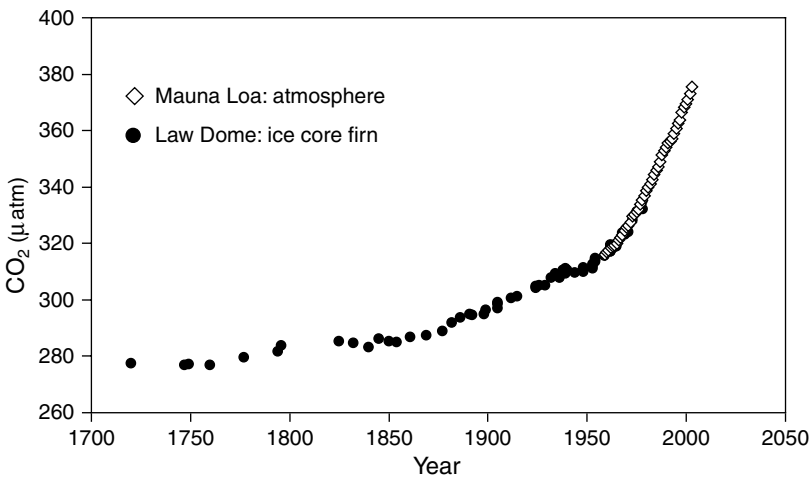

Figure 11.3. The atmospheric CO_2 record at Mauna Loa observatory over the past *c.* 50 years (1958 to present) along with the CO_2 record for pre-industrial time to 1960 as preserved in the Law Dome ice core in East Antarctica.

//FS2/CUP/3-PAGINATION/ERN/2-PROOFS/3B2/9780521833134C11.3D 386 [372–403] 29.1.2008 12:58PM

The likely storage locations for anthropogenic CO_2 are the large global carbon reservoirs that turn over on time periods of decades to centuries. These are DIC in the ocean and organic matter in the terrestrial biosphere (Table 11.1, Fig. 11.1). It is logical that some of the anthropogenic CO_2 put into the atmosphere will invade the ocean by air–sea gas exchange. One might expect the same to be true for the terrestrial biosphere; however, people have had a much greater impact on this carbon reservoir than on that of the ocean. Deforestation releases carbon to the atmosphere and oceans whereas the opposite response, net removal of CO_2 to the terrestrial reservoir, is expected from "greening" of the biosphere. *Greening* refers to anthropogenically enhanced photosynthesis caused by increased atmospheric CO_2 concentrations, fertilization by nutrient loading, or temperature increases. The magnitude of the terrestrial effect is difficult to measure because this reservoir is extremely heterogeneous. Although the ocean's carbon reservoir is more homogeneous, the impact of anthropogenic CO_2 on the DIC is subtle, and only recently have adequate methods been developed to measure the effect.

We begin our discussion of the ocean's role in removal of anthropogenic CO_2 added to the atmosphere by demonstrating the equilibrium chemical response to an atmospheric perturbation and then discuss the methods that have been used to measure the CO_2 uptake by the oceans. Finally, we will demonstrate the role of both the ocean and terrestrial biosphere in sequestering anthropogenic CO_2 during the past 25 years.

11.3.1 The carbonate buffer factor (Revelle factor)

The first stage of describing the role of the ocean in adsorbing anthropogenic CO_2 is to determine the effect of the carbonate equilibrium between the atmosphere and surface waters of the ocean. Since the ocean on average mixes to a depth of about 100 m annually, this part of the ocean's dissolved inorganic carbon reservoir should be nearly in chemical equilibrium with the atmosphere on time scales of one year. The response of the surface ocean carbonate system to changes in f_{CO_2} involves the carbonate buffer system and a number that has come to be known as the "Revelle factor." To demonstrate the response of marine surface water DIC to an increase in atmospheric f_{CO_2}, consider the huge $1\,m \times 1\,m \times 10\,100\,m$ box shown in Fig. 11.4. The box contains $10\,000\,m^3$ of air, V_{atm}, and $100\,m^3$ of seawater, V_{ocean}, and is maintained at a temperature of 20 °C and a pressure of 1 atm at the air–water interface. The seawater inside has an alkalinity, $A_{C\&B}$, of $2300\,\mu eq\,kg^{-1}$ and a DIC concentration of $2000\,\mu mol\,kg^{-1}$. The atmosphere and ocean are at chemical equilibrium. As we learned in Chapter 4, all species of the carbonate system at chemical equilibrium can be computed if two quantities are known. We use the carbonate equilibria described in Chapter 4 and the Matlab program given in Appendix 4.1 to determine that the equilibrium CO_2 concentration in the water is $11.3\,\mu mol\,kg^{-1}$. If the atmosphere and ocean are in solubility equilibrium, Henry's Law can be used to

//FS2/CUP/3-PAGINATION/ERN/2-PROOFS/3B2/9780521833134C11.3D 387 [372–403] 29.1.2008 12:58PM

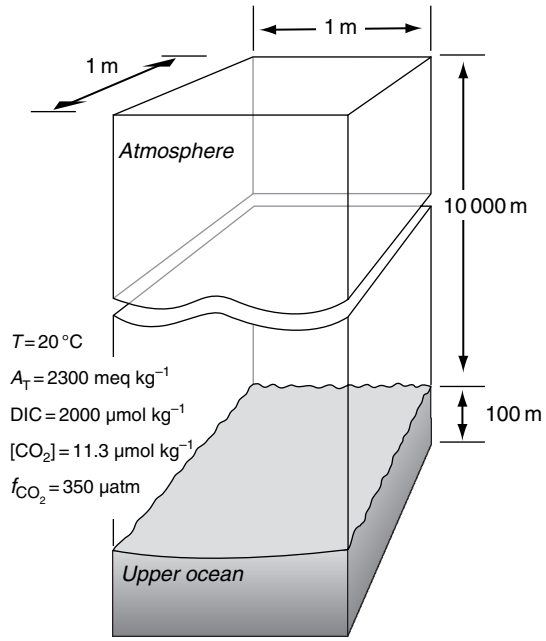

Figure 11.4. Sketch of a tall box with 10 km of air and 100 m of seawater with air and water carbon concentrations indicated. This hypothetical system is used to illustrate the effect of carbonate reactions in controlling the distribution of a perturbation of CO_2 between the atmosphere and ocean at chemical equilibrium.

calculate that the f_{CO_2} of the atmosphere is 350 ppm. The total inventory of carbon in the atmosphere and water in the box in moles is:

$$\sum \mathrm{C} = f^{\mathrm{a}}_{\mathrm{CO_2}} \cdot M_{\mathrm{atm}} + \mathrm{DIC} \cdot V_{\mathrm{ocean}} \cdot \rho, \tag{11.8}$$

where M_{atm} is the number of moles of air in the atmosphere box and ρ (kg l^{-1}) is the density of seawater. If we assume that the pressure at the air–water interface in the box is one atmosphere (1 atm = 101 325 Pascals, Pa or kg m^{-1} s^{-2}), we can calculate the number of moles this represents by dividing by the acceleration due to gravity (9.8 m s^{-2}) and the molecular mass of the atmosphere (0.029 kg mol^{-1}) ($M_{\mathrm{atm}} = 101\,325 / (9.8 \times 0.029) = 3.5 \times 10^5$ mol$_{\mathrm{atm}}$). The total amounts of carbon in the atmosphere and seawater are:

$$\sum \mathrm{C_{atm}} = (0.35 \times 10^{-3}\ \mathrm{mol\,C\,mol^{-1}_{atm}})(3.5 \times 10^5 \mathrm{mol_{atm}}) = 122\ \mathrm{mol\,C}; \tag{11.9}$$

$$\sum \mathrm{C_{DIC}} = (2.0 \times 10^{-3}\ \mathrm{mol\ kg^{-1}})(10^5\,\mathrm{l})(1.023\ \mathrm{kg\,l^{-1}}) = 200\ \mathrm{mol\,C}; \tag{11.10}$$

and the inventory of the CO_2 gas in the water is:

$$\sum \mathrm{C_{SW,CO_2}} = (11.3 \times 10^{-6}\ \mathrm{mol\ kg^{-1}})(10^5\,\mathrm{l})(1.023\ \mathrm{kg\,l^{-1}}) = 1.3\ \mathrm{mol\,C}. \tag{11.11}$$

The amount of carbon in one square meter of seawater 100 m deep is of the same magnitude as that in 10 km of air at 1 atm (compare Eqs. (11.9) and (11.10)), which is analogous to the situation in the real ocean mixed layer and atmosphere.

//FS2/CUP/3-PAGINATION/ERN/2-PROOFS/3B2/9780521833134C11.3D 388 [372–403] 29.1.2008 12:58PM

Now, we inject 20 mol of CO_2 into the atmosphere of the box and ask how the added carbon is distributed between the atmosphere and ocean once the system re-establishes a new chemical equilibrium. If the CO_2 behaved like an inert gas (no chemical reactions) then the added carbon would be distributed following Henry's Law and the fraction of the added carbon that would enter the seawater, f, would be the same as the CO_2 gas distribution in the original equilibrium:

$$f = \frac{\sum C_{SW,\,CO_2}}{\sum C_{atm} + \sum C_{SW,\,CO_2}} = \frac{1.3\ \text{mol}}{122\ \text{mol} + 1.3\ \text{mol}} = 0.010. \tag{11.12}$$

Only 1.0 percent of the CO_2 added would enter the ocean.

If, on the other hand, the added carbon is eventually distributed equally among the dissolved carbon molecules in the water (i.e. the added carbon divides itself among HCO_3^-, CO_3^{2-} and CO_2 so that they have the same fraction of anthropogenic CO_2), then the fraction that enters the seawater would be much greater. This situation is the same as would be expected if a tracer of carbon too small to change the ocean chemistry were added to the atmosphere, say a small amount of $^{14}CO_2$, and allowed to equilibrate with the water. The fraction that would enter the seawater in this case would be:

$$f = \frac{\sum C_{DIC}}{\sum C_{DIC} + \sum C_{atm}} = \frac{200\ \text{mol}}{200\ \text{mol} + 123\ \text{mol}} = 0.62. \tag{11.13}$$

Sixty-two percent of the carbon would end up in the seawater in this scenario.

In fact, neither of these estimates is correct because the amount of carbon that ultimately resides in the seawater is determined by chemical equilibrium in the water; not simply Henry's Law or a tracer-like distribution of the carbon among the constituents of DIC in the water. What we want to know is the equilibrium change in DIC for a given change in f_{CO_2}. This value can be determined from the carbonate equilibrium program in Appendix 4.1 for a given temperature and $A_{C\&B}$ by making small changes in the DIC and determining the change in f_{CO_2}. The change in carbon content of the reservoirs in Fig. 11.4 is given by:

$$\Delta \sum C = \Delta \sum f_{CO_2,\,atm} + \Delta \sum DIC = \Delta f^{a}_{CO_2} M_{atm} + \Delta DIC \times V_{ocean}\ \rho. \tag{11.14}$$

Defining the fraction, f, of the CO_2 taken up by the seawater in the box as the ratio of the changes in the seawater to those in the atmosphere plus seawater gives:

$$f = \frac{\Delta DIC \times V_{ocean}\ \rho}{(\Delta DIC \times V_{ocean}\ \rho) + \left(\Delta f^{a}_{CO_2} M_{atm}\right)}. \tag{11.15}$$

The fractional value can be calculated because we know the relative changes in DIC and $f^{a}_{CO_2}$ at chemical equilibrium for a given $A_{C\&B}$, f_{CO_2}, temperature, and pressure. Pilson (1998) referred to this value as the uptake factor, *UF*:

//FS2/CUP/3-PAGINATION/ERN/2-PROOFS/3B2/9780521833134C11.3D 389 [372–403] 29.1.2008 12:58PM

$$UF = \frac{\Delta \mathrm{DIC}}{\Delta f_{CO_2}} (\mathrm{mol\ kg^{-1}/atm}) \tag{11.16}$$

which is very straightforward and easy to understand, but not very generally usable because of the units. The value was originally presented as a fractional change in DIC and f_{CO_2} at equilibrium by Revelle and Suess (1957) in their classic paper on the fate of fossil fuel CO_2, and later called the Revelle factor, R_{Rev}, by Broecker and Peng (1982):

$$R_{\mathrm{Rev}} = \left(\frac{\Delta f_{CO_2}}{f_{CO_2}}\right) \Big/ \left(\frac{\Delta \mathrm{DIC}}{\mathrm{DIC}}\right). \tag{11.17}$$

Uptake and Revelle factors for the conditions of our experiment in Fig. 11.4 and as a function of f_{CO_2} are presented in Fig. 11.5. For $f_{CO_2} = 350\,\mu\mathrm{atm}$, $UF = 0.6\,\mu\mathrm{mol\,kg^{-1}\,\mu atm^{-1}}$ and $R = 9.6$. Combining Eqs. (11.15) and (11.16) gives:

$$\begin{aligned} f &= \frac{UF \times V_{\mathrm{ocean}}\ \rho}{(UF \times V_{\mathrm{ocean}}\ \rho) + (M_{\mathrm{atm}})} \\ &= \frac{0.6\,\mathrm{mol_{atm} kg^{-1}} \times 100\,\mathrm{m^3} \times 1023\ \mathrm{kg\,m^{-3}}}{0.6\,\mathrm{mol_{atm} kg^{-1}} \times 100\,\mathrm{m^3} \times 1023\ \mathrm{kg\,m^{-3}} + 3.5 \times 10^5 \mathrm{mol_{atm}}} = 0.15. \end{aligned} \tag{11.18}$$

About 15% of the carbon added to the system is ultimately sequestered in the ocean. This is between what would be expected for the cases of the inert gas and tracer distribution among carbon atoms. More CO_2 finds its way into the ocean than in the inert gas case because of the reactions of the carbonate system. Most of the CO_2 that enters the ocean from the atmosphere is consumed by reaction with carbonate ion:

$$CO_2 + CO_3^{2-} + H_2O \leftrightarrow 2HCO_3^-,$$

thereby making way for more CO_2 to enter via gas exchange. In terms of the Revelle factor, a value near $R_{\mathrm{Rev}} = 10$ indicates that the fractional change in f_{CO_2} at equilibrium is about 10 times that of the DIC. Since there is about 200 times more DIC than $[CO_2]$ this represents a carbon uptake by the water that is almost 20 times greater than if there were no chemical reactions.

Notice that in Fig. 11.5 there is a factor of three decrease in *UF* and a 25% decrease in R_{Rev} as the f_{CO_2} increases from preanthropogenic levels of 280 μatm to 550 μatm. The decrease in *UF* indicates a decrease in the efficiency of CO_2 absorption as the f_{CO_2} of the ocean and atmosphere increase. One way to think about the reason for the decreased efficiency is that with decreasing pH the concentration of $[CO_3^{2-}]$ decreases so there is less chemical reaction (see Fig. 4.2).

We can now use the knowledge of the Revelle factor to estimate the anthropogenic CO_2 uptake by the ocean at equilibrium. Presuming that after some reasonable time the ocean carbonate system comes into equilibrium or nearly so with CO_2 in the atmosphere, we can calculate the fraction of the anthropogenic CO_2 taken up by the ocean as a function of the depth of the layer into which

//FS2/CUP/3-PAGINATION/ERN/2-PROOFS/3B2/9780521833134C11.3D 390 [372–403] 29.1.2008 12:58PM

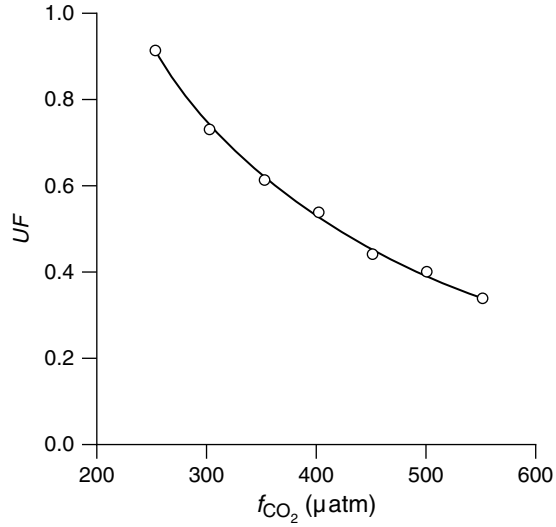

Figure 11.5. The change in the uptake factor (*UF*) and Revelle factor (*R*) as a function of the f_{CO_2} in equilibrium with a seawater solution containing a total alkalinity of 2300 $\mu eq\,kg^{-1}$.

f_{CO_2} (μatm)	DIC (μmol kg^{-1})	$[CO_3^{2-}]$ (μmol kg^{-1})	pH_T	*UF* (μmol kg^{-1} μatm^{-1})	*R*
250	1928	264	8.21	0.90	8.6
300	1968	234	8.15	0.72	9.1
350	2000	216	8.10	0.60	9.6
400	2028	199	8.05	0.52	10.1
450	2051	184	8.00	0.43	10.6
500	2071	171	7.96	0.38	11.0
550	2088	160	7.93	0.33	11.5

anthropogenic CO_2 has equilibrated, h, following exactly the reasoning in the above experiment. The fraction of anthropogenic CO_2 in the ocean is:

$$f_{\text{ocean}} = \frac{\sum_{\text{ocean}} \times (\Delta \text{DIC}_{\text{anthro}}/\text{DIC})}{\sum_{\text{atmos}} \times (\Delta f_{CO_2,\ \text{anthro}}/f_{CO_2}) + \sum_{\text{ocean}} \times (\Delta \text{DIC}_{\text{anthro}}/\text{DIC})}, \tag{11.19}$$

where Σ_{ocean} is the ocean inventory of DIC and Σ_{atmos} is the atmospheric inventory of CO_2:

$$\begin{aligned} \sum_{\text{ocean}} &= [\text{DIC}] \times \text{area}_{\text{ocean}} \times h = \left(2\,\text{mol}\,\text{m}^{-3}\right)\left(3.6 \times 10^{14}\text{m}^2\right)h \\ &= 7.2 \times 10^{14}\,\text{mol} \times h. \end{aligned} \tag{11.20}$$

$$\begin{aligned} \sum_{\text{atmos}} &= \text{mol}\,CO_2\,(\text{mol}\,\text{atm})^{-1} \times (\text{mol atm}) \\ &= \left(350 \times 10^{-6}\ \text{mol}\,CO_2\,(\text{mol atm})^{-1}\right)\left(1.77 \times 10^{20}\ \text{mol}\,\text{atm}\right) \\ &= 6.2 \times 10^{16}\,\text{mol}\,\text{C}. \end{aligned} \tag{11.21}$$

Using the definition of the Revelle factor and rearranging:

//FS2/CUP/3-PAGINATION/ERN/2-PROOFS/3B2/9780521833134C11.3D 391 [372–403] 29.1.2008 12:58PM

$$f_{\text{ocean}} = \frac{\sum \text{ocean}}{\sum \text{atmos} \cdot R_{\text{Rev}} + \sum \text{ocean}} = \frac{7.2 \times 10^{14}\, h}{6.2 \times 10^{16} \cdot R + 7.2 \times 10^{14}\, h}. \tag{11.22}$$

This fraction is plotted as a function of the layer depth, h, in Fig. 11.6. As the mean depth of the ocean mixed layer is on the order of 100 m, we see from the plot that at chemical equilibrium the surface ocean will take up approximately 10% of the CO_2 added to the atmosphere. This is nearly the same as that calculated in the box analogy and might be viewed as an absolute lower limit of the amount of anthropogenic CO_2 that penetrates the ocean because the global average mixed layer depth is about 100 m. It is clear that in some areas of the oceans transient tracers such as bomb-produced ^{14}C and ^{3}H (with even shorter life times than fossil fuel CO_2), have penetrated through the mixed layer well into the thermocline (see Fig. 5.16). In order for the ocean to take up half of the fossil fuel CO_2 (roughly that amount missing from the atmosphere) the upper 700–800 m of the ocean would have to be in equilibrium with the atmosphere (Fig. 11.6). Thus, the limiting factor for the uptake of fossil fuel CO_2 by the ocean is the rate of mixing into the thermocline rather than gas exchange or the approach to chemical equilibrium in the water.

We have so far assumed that the atmosphere and ocean are in equilibrium. This of course cannot be the case, as the CO_2 content of the atmosphere is rising rapidly, so there must be a gradient in f_{CO_2} across the air–water interface to drive the flux into the ocean. The concepts of the Revelle and uptake factors are also useful in determining the response time of the upper ocean to perturbations of gas and isotope changes in the atmosphere. As discussed in Chapter 2, the residence time of a substance is equal to its reservoir size divided by the flux in or out. For an inert gas, C, in the upper ocean the time for (1–1/e) of the gas to be exchanged by flux across the air–water

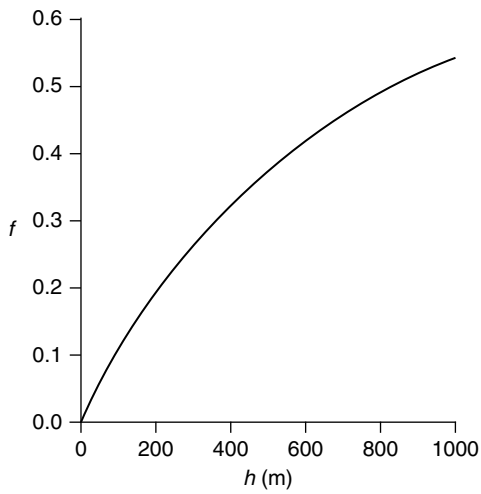

Figure 11.6. The fraction, f, of CO_2 added to the surface ocean–atmosphere system that would go into the ocean as a function of the depth, h, of the ocean surface layer that is in equilibrium with atmospheric f_{CO_2}.

//FS2/CUP/3-PAGINATION/ERN/2-PROOFS/3B2/9780521833134C11.3D 392 [372–403] 29.1.2008 12:58PM

interface is the concentration, [C], times height, h, of the mixed layer divided by the one-way gas exchange flux:

$$\tau_{\text{inert}} = \frac{h \cdot [\text{C}]}{F_{\text{air-water}}} = \frac{h \cdot [\text{C}]}{G \cdot [\text{C}]} = \frac{h}{G}, \tag{11.23}$$

where G is the gas exchange mass transfer coefficient and has units of length / time (Chapter 10). We use the one-way flux because all the gases are being exchanged, not just the fraction that is over- or undersaturated. Even in a situation where the air and ocean are exactly in saturation equilibrium, gases in each reservoir will have a finite residence time with respect to exchange. Using a mean gas exchange mass transfer coefficient of $5\,\text{m}\,\text{d}^{-1}$ and an ocean mixed layer depth of 100 m results in a residence time of 20 d (less than one month). If CO_2 were an inert gas this would be the residence time:

$$\tau_{\text{inert}} = \frac{h}{G} = \frac{100}{5} = 20 \text{ d}. \tag{11.24}$$

The true reservoir size for carbon dioxide, however, is larger than its concentration, $[CO_2]$, because of the carbonate system reactions. The ratio of the reservoir of DIC that exchanges carbon to the CO_2 gas reservoir in the mixed layer is $\Delta\text{DIC}/\Delta[CO_2]$. Thus, the residence time for carbon in the surface ocean with respect to gas exchange from Eq. (11.23) is:

$$\tau_{CO_2} = \frac{h[CO_2]}{G[CO_2]} \times \frac{\Delta\text{DIC}}{\Delta[CO_2]} = \frac{h}{G}\left(\frac{\text{DIC}}{R[CO_2]}\right) = 20\left(\frac{\text{DIC}}{R[CO_2]}\right), \tag{11.25}$$

where the value in the last term was taken from the Revelle factor equation (11.16), by substituting $[CO_2]$ for f_{CO_2}.

Using values of DIC, R, and $[CO_2]$ for the case in Fig. 11.4:

$$\tau_{CO_2} = 20 \times 18.4 = 368 \text{ d}. \tag{11.26}$$

The renewal time is about one year for a mixed layer 100 m deep! This indicates that the surface ocean anthropogenic increase should lag that in the atmosphere, but not by much because the anthropogenic perturbation is a decadal to centuries-long process.

One can also estimate the renewal time for the isotopes of carbon, ^{13}C and ^{14}C, by using this simple reasoning. The response time will be different again because isotopes must exchange with the entire carbon reservoir. This reasoning follows that for the tracer case described earlier (Eq. (11.13)), since the individual carbon molecules are tagged with their isotope signature, and we are asking how long it takes for the ^{13}C of the DIC to come to a new steady state in which the entire DIC reservoir must be considered. Thus,

$$\tau_{\text{isotope}} = \frac{h \cdot [\text{DIC}]}{G \cdot [CO_2]} = \frac{20 \times [\text{DIC}]}{[CO_2]} = 20 \times 177 = 3540 \text{ d}. \tag{11.27}$$

The response time for the upper ocean with respect to changing its isotopic values is about ten times longer than that for CO_2 and almost

//FS2/CUP/3-PAGINATION/ERN/2-PROOFS/3B2/9780521833134C11.3D 393 [372–403] 29.1.2008 12:58PM

200 times that for an inert gas ($\tau_{\text{isotope}} = 10$ y!) because of the size of the DIC reservoir relative to the rate of CO_2 gas transfer.

11.3.2 Methods of measuring anthropogenic CO_2 uptake

Estimates of the amount of anthropogenic CO_2 presently in the ocean have been determined in four main ways. The first method is to distinguish the fraction of the measured DIC increase that comes from invasion of anthropogenic CO_2. This is accomplished by calculating the natural increase in DIC with depth from nutrient and oxygen data with the assumption of constant metabolic ratios. The difference between the calculated value and that measured is the anthropogenic perturbation. The second method involves calculation of the present-day global flux of CO_2 across the ocean–atmosphere interface from observations of the degree of saturation of f_{CO_2} and estimates of gas transfer velocities. This calculation involves global measurements of the CO_2 fugacity in surface waters, $f^{w}_{CO_2}$, and represents a present-day flux rather than an inventory. This method is less accurate than the others because of the temporal and spatial variability of surface ocean f_{CO_2}, but for the same reason it provides valuable information about locations and mechanisms of anthropogenic CO_2 uptake. The third method uses the observation that the $\delta^{13}C$ of fossil fuel CO_2 is much different from that found naturally in the ocean and atmosphere. Changes in $\delta^{13}C$ in seawater can be used to trace the fraction of the DIC that has been anthropogenically introduced. Finally, one can calculate (as opposed to measure) the oceanic burden of anthropogenic CO_2 in global circulation models by releasing CO_2 into the model atmosphere of a GCM and determining the amount that invades the model ocean.

The first of the direct measurement methods has been the most successful for determining the amount and location of anthropogenic CO_2 in the ocean at the time of writing this book. In this method the DIC increases below the surface mixed layer due to anthropogenic contamination and natural metabolic processes are distinguished. The technique was first applied by Brewer (1978) and Chen and Millero (1979) in its simplest form. In this early version, measured DIC values were subtracted from calculated natural (uncontaminated by anthropogenic CO_2) DIC values as a function of depth or age along a constant density surface. Natural DIC values at some depth, x, $DIC_{N,x}$, are equal to the preanthropogenic value at the surface, $DIC_{N,0}$, plus that from organic matter degradation and calcium carbonate dissolution:

$$DIC_{N,x} = DIC_{N,0} - r_{DIC:O_2} \cdot AOU_x + \tfrac{1}{2}\left(A_{T,x} - A_{T,S} + r_{NO_3:O_2} \cdot AOU_x\right). \tag{11.28}$$

The stoichiometric ratios $r_{DIC:O_2}$ and $r_{NO_3:O_2}$, convert the oxygen deficit caused by organic matter degradation to DIC and nitrate increase, respectively (both negative values). The terms on the right side represent, in order, the value of the DIC at the surface before

//FS2/CUP/3-PAGINATION/ERN/2-PROOFS/3B2/9780521833134C11.3D 394 [372–403] 29.1.2008 12:58PM

it changed due to anthropogenic effects, the increase in DIC at location x below the surface layer due to organic matter degradation, and the increase in DIC at location x due to calcium carbonate dissolution. The value in parentheses in the last term is the alkalinity change, represented by the measured difference between the value at location x and surface waters, $(A_{T,x} - A_{T,S})$, minus ($r_{NO_3:O_2}$ is negative) the alkalinity decrease by oxidation of NH_3 from organic matter to NO_3^- (see Section 4.4.2). The anthropogenic component of the measured DIC is the difference between measured value and DIC_N.

$$DIC_{anthro} = DIC_{meas,x} - DIC_{N,x}. \tag{11.29}$$

To use this equation, one has to have a scheme for evaluating the surface ocean DIC and alkalinity before anthropogenic contamination. If you know the surface alkalinity, the DIC at chemical equilibrium can be calculated from T, S, and $f_{CO_2} = 280$ ppm (the preanthropogenic value). Alkalinity at the surface is evaluated by either assuming it is equal to present values or calculating it from present correlations with surface salinity and the measured salinity value. This is the weakest aspect of the method because it assumes that f_{CO_2} in the surface water was at equilibrium with the atmosphere and there may also be complications due to mixing of several different water masses. Gruber *et al.* (1996) developed new ways to address these uncertainties and improved the accuracy of this approach. The method has been subsequently applied to the world's ocean basins. An estimate of the invasion of anthropogenic CO_2 calculated in this way is presented in Fig. 11.7. The value in near-surface waters is 40–50 μmol kg^{-1} or about 2% of the total DIC.

Anthropogenic contamination reaches the ocean bottom in the northern part of the North Atlantic because of the deep convection of the North Atlantic Deep Water. Further south in the basin the contamination reaches to depths of 2000 m. The depth at which the profiles reach half their surface maximum is between 600 and 1000 m. Note that this depth is not greatly different from the value of 800 m estimated in Fig. 11.6 for the depth of ocean equilibrium required to accommodate about half of the fossil fuel released to the atmosphere. It has been shown with global circulation models that a present-day flux of 2.2 Pg y^{-1} into the ocean is required to accommodate the inventory of CO_2 indicated in Fig. 11.7 (Table 11.3).

The second method of determining the anthropogenic uptake of CO_2 is accomplished by calculating the flux across the air–water interface. Takahashi *et al.* (2002) have compiled more than half a million sea-surface f_{CO_2} measurements from different years and seasons. They normalized these measurements into a composite year with different seasons and extrapolated the data to fill in regions with little data coverage by using a surface ocean circulation model. These "climatological" f_{CO_2} results are multiplied by the gas exchange mass transfer coefficient, G_{CO_2}, which is calculated from correlations

//FS2/CUP/3-PAGINATION/ERN/2-PROOFS/3B2/9780521833134C11.3D 395 [372–403] 29.1.2008 12:58PM

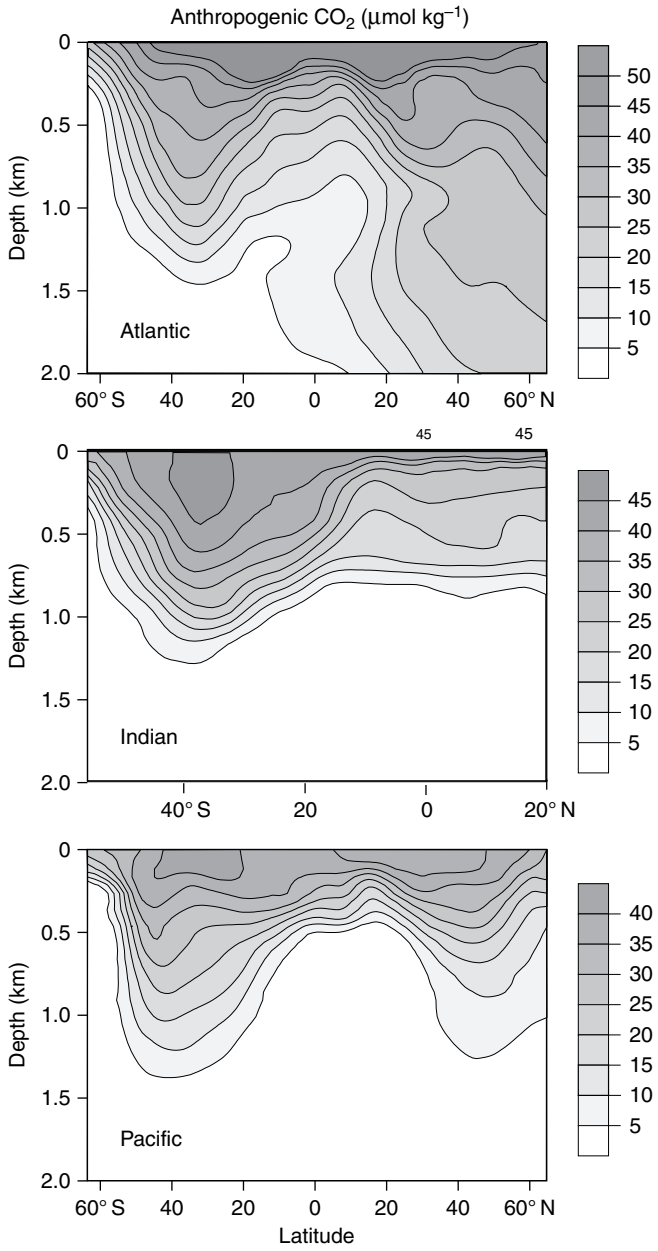

Figure 11.7. A cross section of the anthropogenic CO_2 in the ocean determined from ocean DIC by the method described in the text. Robert Key, personal communication; Key *et al.* (2004).

to wind speed for different seasons and regions (see Chapter 10) to determine the global flux of CO_2 into the ocean:

$$F_{CO_2} = G_{CO_2} \cdot K_H \cdot \left(f^{a}_{CO_2} - f^{SO}_{CO_2} \right) \tag{11.30}$$

where K_H is the Henry's Law coefficient. A map of the global distribution of the air–water CO_2 fluxes calculated in this way is presented in Fig. 11.8. The important areas of CO_2 evasion to the atmosphere are the Equator (particularly the Eastern Equatorial Pacific) and the NW

//FS2/CUP/3-PAGINATION/ERN/2-PROOFS/3B2/9780521833134C11.3D 396 [372–403] 29.1.2008 12:58PM

Table 11.3. *Estimates of anthropogenic carbon dioxide uptake rate by the oceans*

Method of determination	Flux (Pg y^{-1})
Experimental results	
Ocean inventory: DIC[a]	2.2
Gas exchange (1995)[b]	2.2 ± 0.4
δ^{13}C-DIC inventory (1970–1990)[c]	1.7 ± 0.2
(1980s)	2.0 ± 0.2
Atmospheric measurements: O_2/N_2, CO_2 (1990–2000)	1.7 ± 0.5[d]
O_2/N_2, CO_2, δ^{13}C-CO_2 (1991–1997)[e]	2.0 ± 0.6
Model results (1980–1989)	
Range of four different global models[f]	1.5 to 2.2

[a] The DIC method produces a global inventory, not a flux. The inventory is 118 Pg C (Sabine *et al*., 2004) . This is assigned a flux by analogy with a GCM inventory of 118 Gt that results from an annual flux of 2.2 Gt CO_2 y^{-1} (Orr *et al*., 2000).
[b] Takahashi *et al.* (2002).
[c] Quay *et al*. (1992, 2003).
[d] IPCC (2001).
[e] Battle *et al*. (2000).
[f] Values of the four different models are 2.2, 2.1, 1.6, and 1.5 (Orr *et al*., 2000).

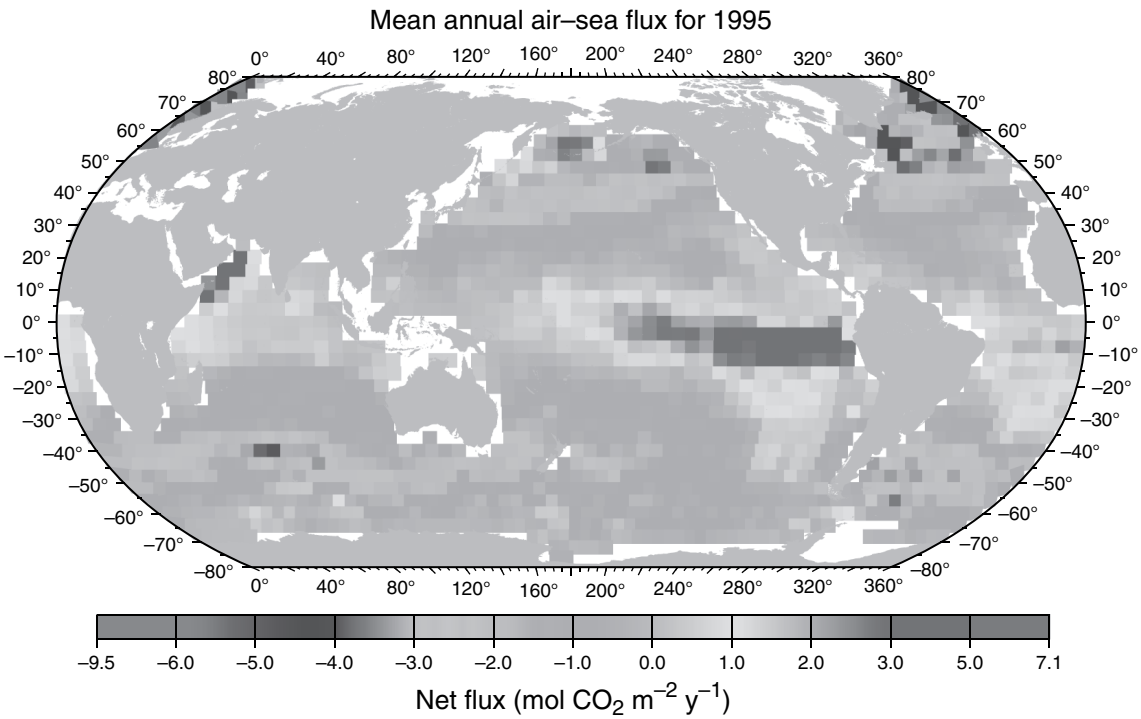

Figure 11.8. The mean annual flux of CO_2 between the atmosphere and ocean, based on measurements of f_{CO_2} in the ocean and atmosphere, and the gas exchange mass transfer coefficient determined from wind speed. From Takahashi *et al.* (2002). (See Plate 8.)

//FS2/CUP/3-PAGINATION/ERN/2-PROOFS/3B2/9780521833134C11.3D 397 [372–403] 29.1.2008 12:58PM

Indian Ocean. These are regions of upwelling from deeper waters that are enriched in CO_2. The subtropical oceans are about in equilibrium with the atmospheric f_{CO_2} and carbon dioxide invades strongly in the North and South Pacific and Atlantic north of about 40° N. Cooling of both the Kuroshio and Gulf Stream in the Northern Hemisphere plays an important role in the carbon dioxide uptake at the gyre boundaries because CO_2 becomes undersaturated as these grand ocean currents move northward and across the oceans. CO_2 undersaturation caused by cooling and carbonate thermodynamics, however, is not the whole story. It has been shown that mixing at the gyre boundaries brings nutrients to the surface, enhancing biological productivity that aids in the f_{CO_2} drawdown in these regions. Regional and seasonal f_{CO_2} atmosphere–ocean differences range from $>100\,\mu$atm supersaturated to $>100\,\mu$atm undersaturated, so even with the large data coverage there is a considerable error in the calculated annual flux. There are also uncertainties associated with the estimate of the mass transfer coefficient from global wind speeds, particularly at high winds (see Chapter 10). At the time of writing this book the best estimate of the mean net invasion rate with this method is 2.2 ± 0.4 Pg y^{-1} (Takahashi *et al.*, 2002) (Table 11.3). The global mean degree of surface water undersaturation of f_{CO_2} to supply 2.0 Pg y^{-1} of carbon to the oceans is 8 μatm. The most important regions of ocean uptake of anthropogenic CO_2 are different from locations where it accumulates (based on the DIC method). Regions where uncontaminated deep water reaches the surface – high latitudes, the Equator and the subtropical/subarctic frontal regions – are the areas of most anthropogenic CO_2 uptake. Relatively little CO_2 enters the ocean thermocline in the subtropical regions but this is the ocean location where much of the anthropogenic CO_2 is stored. Circulation tends to pool this transient tracer in these locations (notice the large inventories in these areas in Fig. 11.7).

The third experimental method for determining the anthropogenic burden in the ocean involves global data for changes in the carbon isotope ratio of the DIC of the ocean and CO_2 of the atmosphere. Because the $\delta^{13}C$ of fossil fuel CO_2 is about –23% and that of the DIC of the ocean is near zero, contamination of the carbon isotope ratio of CO_2 in the atmosphere and DIC in the oceans is readily measurable. This is demonstrated by comparing the $\delta^{13}C$-DIC in the surface oceans between 1970 and 1990 (Fig. 11.9). Quay *et al.* (1992) introduced this method by compiling measurements of the $\delta^{13}C$ in the atmosphere and ocean between 1970 and 1990 and calculating the air–sea flux necessary to account for the measured differences. The method is sensitive to the $\delta^{13}C$ fractionation factor during gas exchange and accurate measurements from past global surveys (GEOSECS in the 1970s), which in some cases are problematic. Using this method, Quay *et al.* (2003) estimate an ocean uptake rate of 2.0 ± 0.2 Pg y^{-1} during the period 1970–1990 (Table 11.3).

Models have been used to estimate the uptake of anthropogenic CO_2 since well before the experimental procedures were of good

//FS2/CUP/3-PAGINATION/ERN/2-PROOFS/3B2/9780521833134C11.3D 398 [372–403] 29.1.2008 12:58PM

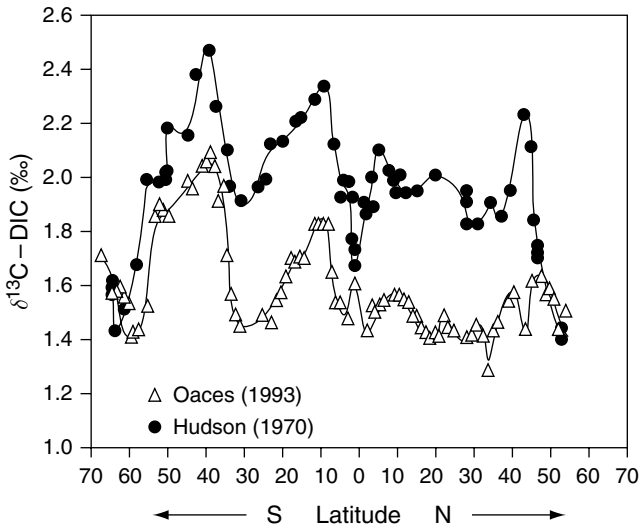

Figure 11.9. The carbon isotope ratio of DIC in the surface of the Pacific Ocean. The data illustrate how the value has decreased between 1970 and 1991 owing to the addition of fossil fuel CO_2 to the atmosphere. Oaces (1993) and Hudson (1970) refer to two different ocean cruises. From Quay *et al.* (2003).

enough quality to accurately measure the changes. We have shown by the equilibrium calculations and the measured penetration depths that the limiting factor for oceanic anthropogenic CO_2 uptake is mixing of water across the thermocline. It is thus extremely important for the mixing rates of the models to be calibrated by matching the penetration of other transient tracers (^{14}C, ^{3}H, and CFCs) into the ocean. Once this is accomplished, the models are run for several hundred years while CO_2 is delivered to the atmosphere according to the anthropogenic usage. To date, estimates for the CO_2 uptake rate employing different models have been made to date with values ranging from 1.5 to 2.3 Pg y^{-1}. These results are presented along with estimates of the experimental methods in Table 11.3. The average and standard deviation of the means of all the model and experimental estimates is 1.9 ± 0.2. The relatively tight concurrence among the different techniques indicates that the rate of anthropogenic CO_2 uptake in the ocean over the past several decades is reasonably well known.

The critical unknowns in this field have evolved in the past 20–30 y from what the anthropogenic carbon fluxes are, to understanding the mechanisms controlling the ocean's CO_2 pumps and anthropogenic CO_2 uptake. These tasks utilize both interdisciplinary experimental observations and global circulation models. If the models can be made to accurately reproduce experimentally determined fluxes and storage patterns, then it should be possible to accurately predict the response to future changes.

11.3.3 Partitioning anthropogenic CO_2 among the ocean, atmosphere, and terrestrial reservoirs

For many years it was assumed that tropical deforestation was a significant source of CO_2 to the atmosphere (between 10% and half of the source from fossil fuel combustion). When these sources were combined with the relatively well-known sinks in the atmosphere

//FS2/CUP/3-PAGINATION/ERN/2-PROOFS/3B2/9780521833134C11.3D 399 [372–403] 29.1.2008 12:58PM

Table 11.4. *Carbon budget for 1980s*

Positive values are sources to the atmosphere. Negative values are sinks. Notice that had the value from deforestation been assumed to be zero the budget would have balanced.

Source or sink	Pg C y^{-1}
Emissions from fossil fuel combustion	$+5.4 \pm 0.5$
Emissions from deforestation and land use	$+1.6 \pm 1.0$
Atmospheric accumulation	-3.2 ± 0.2
Uptake by the ocean	-2.0 ± 0.6
Net imbalance	$\mathbf{+1.8 \pm 1.3}$

Source: From Siegenthaler and Sarmiento (1993).

and ocean, there was a significant excess source. An example of this balance sheet is shown in Table 11.4. While the source from the terrestrial biosphere was uncertain it none the less was assumed to be positive because of known global deforestation. This uncertainty stood until it was demonstrated that with simultaneous determinations of the increase in atmospheric f_{CO_2} and decrease in f_{O_2} it was possible to identify the difference between the global terrestrial biosphere and ocean sinks (Keeling *et al.*, 1996). One might at first expect that these two tracers are redundant because there is an exact stoichiometry between CO_2 release and O_2 consumption by organic matter combustion. The difference, however, is that while both the land and ocean represent potential sinks (or sources) for CO_2 in response to the anthropogenic perturbation, the ocean does not significantly exchange oxygen in response to the anthropogenic decrease in atmospheric O_2. Because O_2 is a very insoluble gas, about 95% of the global reservoir is in the atmosphere. Thus, when atmospheric O_2 decreases owing to fossil fuel burning, there is not a significant subsequent release of O_2 from the ocean to make up the deficit in the atmosphere. Any change in the atmospheric O_2 concentration other than that due to fossil fuel combustion must be attributed to exchange with the terrestrial biosphere.

Calculation of the importance of ocean, atmosphere, and terrestrial biosphere to the anthropogenic CO_2 source was first presented graphically (Keeling *et al.*, 1996). An updated version (Fig. 11.10) (IPCC, 2001) shows the measured decrease in atmospheric oxygen versus the simultaneous increase in atmospheric CO_2 during the 1990s, culminating in a ratio indicated by the filled circle at the year 2000 on the figure. Since the carbon and hydrogen content of the three main fossil fuel sources during this period are known along with their relative consumption rates, an accurate composite of the oxygen demand to carbon dioxide source can be determined. The fossil fuel mixture presently being mined (Table 11.5) results in an oxygen to CO_2 atmospheric change of $\Delta O_2 / \Delta CO_2 = -1.45$. Because the total amount burned and its ΔO_2:ΔCO_2 ratio are known, the line

//FS2/CUP/3-PAGINATION/ERN/2-PROOFS/3B2/9780521833134C11.3D 400 [372–403] 29.1.2008 12:58PM

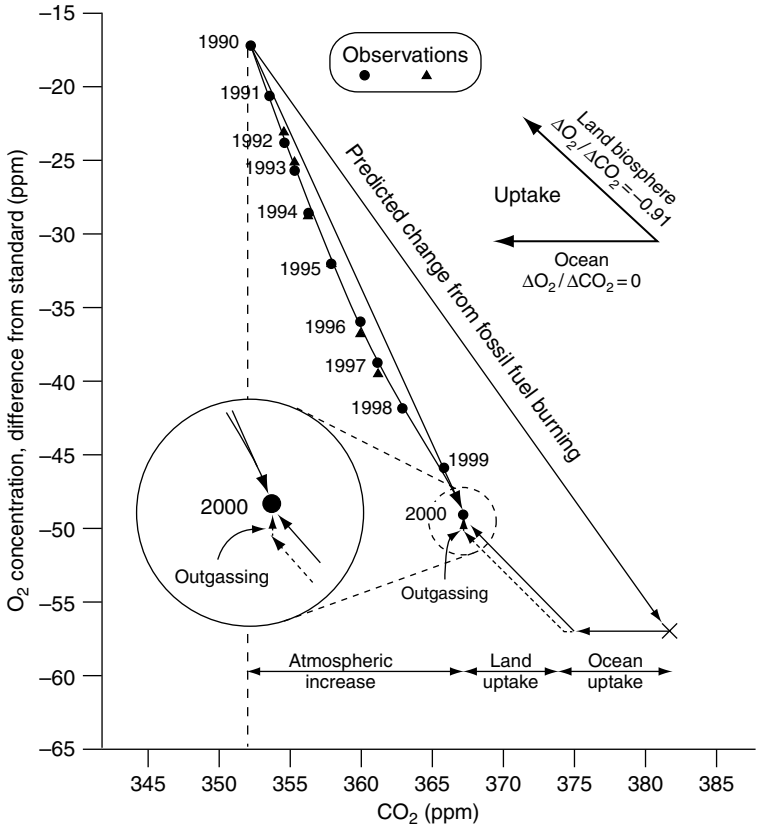

Figure 11.10. The mean change in the atmospheric O_2 and CO_2 partial pressures (ppm) for the period of the 1990s, and illustration of its utility in determining anthropogenic CO_2 uptake by the ocean and land. Symbols are observations between 1990 and 2000. The long diagonal line from the upper left to the lower right is the trend expected, given the amount of fossil fuels burned, if there were no land or ocean exchange. The horizontal line in the lower right corner indicates ocean–atmosphere exchange of CO_2, and the short diagonal line that trends to the upper left from where the horizontal line stops illustrates the trend for uptake of CO_2 and release of O_2 with the land reservoir (see text). Solid lines indicate the trends expected were there no non-steady-state "outgassing" of O_2 from the ocean. Dashed lines and the close-up indicate how the steady-state picture is altered by non-steady-state outgassing of O_2 from the ocean because of changes in ocean ventilation and seawater temperature. Modified from IPCC (2001).

labeled "fossil fuel burning" represents the projected atmospheric change if there were no exchange with the ocean or atmosphere between 1900 and 2000 ending at the location indicated by the (X). Clearly this line is quite different from the observations, reflecting the response of the terrestrial and oceanic reservoirs. The ΔO_2:ΔCO_2 uptake ratio for land biota–atmosphere interaction is $= -1.1$, and this ratio for the ocean–atmosphere interaction is approximately zero. Thus, there are two straight-line paths with known ΔO_2:ΔCO_2 ratios by which we can connect the year 2000 prediction in Fig. 11.10 (X) to the observed value (filled circle). Drawing the only possible straight line paths between the expected and observed values involves quantifying both the oceanic and the atmospheric sinks.

This procedure is simple and elegant and relies on the atmosphere to homogenize the globally heterogeneous fluxes of oxygen and CO_2. The result is (Table 11.1) (IPCC, 2001) that of the $+6.3$ Pg y^{-1} of anthropogenic CO_2 produced during the 1990s, $+3.2$ Pg y^{-1} remained in the atmosphere, -1.7 Pg y^{-1} went into the ocean and -1.4 Pg y^{-1} was taken up by the terrestrial biosphere. During the period of this investigation, the land, rather than being a source to the atmosphere because of deforestation, was a sink because of forest regrowth and enhanced growth due to increased atmospheric CO_2!

//FS2/CUP/3-PAGINATION/ERN/2-PROOFS/3B2/9780521833134C11.3D 401 [372–403] 29.1.2008 12:58PM

Table 11.5. *Carbon and oxygen stoichiometry of fossil fuel burning*

Source	Reaction	$\Delta O_2/\Delta CO_2$
Coal	$2\ C_{10}H_6 + 23\ O_2 \rightarrow 20\ CO_2 + 6\ H_2O$	23/20
Oil	$2\ CH_2 + 3\ O_2 \rightarrow 2\ CO_2 + 2\ H_2O$	3/2
Natural gas	$CH_4 + 2\ O_2 \rightarrow CO_2 + 2\ H_2O$	2/1

Source: Keeling *et al*. (1996).

One cannot compare this result with that in Table 11.4 because they represent different time periods. Analysis of atmospheric changes in CO_2, $O_2 : N_2$ ratio, and the $\delta^{13}C$ of the CO_2 for the period of the 1980s and 1990s (Battle *et al*., 2000) indicates that the role of the terrestrial biosphere during the 1980s and 1990s has been very different. During the 1980s it was about neutral, i.e. any source to the atmosphere via deforestation was nearly matched by uptake due to enhanced new forest growth. In the 1990s global greening dominated the terrestrial signal. Thus, the original balance sheet in Table 11.4 indicates no imbalance at all. The estimates of the role of the biosphere when this table was published appear to have been inaccurate. There is presently no indication that there is a missing sink for fossil fuel CO_2; however, recent atmospheric studies indicate that the role of the biosphere has rapidly changed in a matter of one to two decades from being neutral to becoming a very large sink. This is presently believed to be due to a large recent increase in forest regrowth on land; however, the rapidity of the change was a surprise and will be the subject of intense research in decades to come.

A note of caution is in order before concluding this chapter. The calculations illustrated by Fig. 11.10 here are not bullet-proof. One of the assumptions in the calculation has been that the natural background ocean–atmosphere exchange of gases is at steady state. It is becoming clear that this is probably not the case. It is known that the temperature of ocean surface waters is increasing (decreasing its ability to store oxygen), and repeat hydrography sections in many regions of the ocean indicate decadal-scale decline in the oxygen content of the upper thermocline between the 1980s and 1990s, presumably because of a decrease in the ventilation of thermocline waters (e.g. Fig. 6.23). If there is a net oxygen flux out of the ocean to account for the decreasing oxygen content of the thermocline and the warming of surface waters it will require an additional arrow in Fig. 11.10. This arrow is vertical because it represents a non-steady-state "degassing" of O_2 from the ocean to the atmosphere. (There is also a degassing of CO_2 associated with the non-steady-state warming, but this part of the ocean exchange is already accounted for by the horizontal line indicating CO_2 uptake by the ocean.) The seemingly small correction for the non-steady-state process has a significant effect on the estimates of ocean and terrestrial CO_2 uptake. As indicated by the dashed arrow in Fig. 11.10, the effect of this

//FS2/CUP/3-PAGINATION/ERN/2-PROOFS/3B2/9780521833134C11.3D 402 [372–403] 29.1.2008 12:58PM

additional flux is to increase the uptake estimates of CO_2 by the ocean and decrease the CO_2 sequestration by land. A minimum estimate of this effect is the observed increase in temperature of the surface ocean during the 1990s. A larger estimate is derived from GCM models that analyze the O_2 "degassing" effect of global warming (e.g. Bopp *et al.*, 2002). The accurate value for this effect is presently uncertain, but even the upper estimates are not large enough to account for the very large differences in land and ocean sequestering suggested for the decades of the 1980s and 1990s.

References

Archer, D. E., G. Eschel, A. Winguth *et al.* (2000) Atmospheric pCO_2 sensitivity to the biological pump in the ocean. *Global Biogeochem. Cycles* **14**, 1219–30.

Battle, M., M. L. Bender, P. P. Tans *et al.* (2000) Global carbon sinks and their variability inferred from atmospheric O_2 and del^{13}C. *Science* **287**, 2467–70.

Berner, R. A. (1990) Atmospheric carbon dioxide levels over Phanerozoic time. *Science* **249**, 49–75.

Bopp, L., C. Le Quere, M. Hmann and A. C. Manning (2002) Climate-induced oceanic oxygen fluxes: implications for the contemporary carbon budget. *Global Biogeochem. Cycles* **16**, 2, doi: 10.1029/2001GB001445.

Brewer, P. G. (1978) Direct observation of the oceanic CO_2 increase. *Geophys. Res. Lett.* **4**, 997–1000.

Broecker, W. S. (1971) A kinetic model for the chemical composition of sea water. *Quat. Res.* **1**, 188–207.

Broecker, W. S. and T.-H. Peng (1982) *Tracers in the Sea*. Lamont-Doherty Earth Observatory.

Chen, C. T. and F. J. Millero (1979) Gradual increase of oceanic carbon dioxide. *Nature* **277**, 205–6.

Eppley, R. W. and B. J. Peterson (1979) Particulate organic matter flux and planktonic new production in the deep ocean. *Nature* **282**, 677–80.

Gruber, N., J. L. Sarmiento and T. F. Stocker (1996) An improved method for detecting anthropogenic CO_2 in the oceans. *Global Biogeochem. Cycles* **10**, 809–7.

IPCC (2001) *Climate Change 2001: The Scientific Basis*. Contributions of Working Group I to the third assessment report of the intergovernmental panel on climate change (ed. J. T. Houghton, Y. Ding, D. J. Griggs *et al.*). Cambridge: Cambridge University Press.

Keeling, C. D. (1960) The concentration and isotopic abundance of CO_2 in the atmosphere. *Tellus* **12**, 200–3.

Keeling, R. F., S. C. Piper and M. Heinmann (1996) Global and hemispheric CO_2 sinks deduced from changes in atmospheric O_2 concentration. *Nature* **381**, 218–21.

Key, R. M., A. Kozar, C. L. Sabine *et al.* (2004) A global ocean carbon climatology: results from Global Data Analysis Project (GLODAP). *Global Biogeochem. Cycles* **18**, GB4031, doi: 10.1029/2004GB002247.

Orr J. C., *et al.* (2000) Estimates of anthropogenic carbon uptake from four three-dimensional global ocean models. *Global Biogeochem. Cycles* **15**, 43–60.

Pilson, M. E. Q. (1998) *An Introduction to the Chemistry of the Sea*. Englewood Cliffs, NJ: Prentice-Hall.

//FS2/CUP/3-PAGINATION/ERN/2-PROOFS/3B2/9780521833134C11.3D 403 [372–403] 29.1.2008 12:58PM

Quay, P. D., R. Sonnerup, T. Westby, J. Stutsman and A. McNichol (2003) Changes of the $^{13}C/^{12}C$ of dissolved inorganic carbon in the ocean as a tracer of anthropogenic CO_2 uptake. *Global Biogeochem. Cycles* **17**, 1, doi: 10.1029/2001GB001817.

Quay, P. D., B. Tilbrook and C. S. Wong (1992) Oceanic uptake of fossil fuel CO_2: carbon-13 evidence. *Science* **256**, 74–9.

Revelle, R. and H. E. Suess (1957) Carbon dioxide exchange between atmosphere and ocean and the question of an increase of atmospheric CO_2 during past decades. *Tellus* **9**, 18–27.

Sabine, C. *et al.* (2004) The ocean sink for anthropogenic CO_2. *Science* **305**, 367–71.

Siegenthaler, U. and J. L. Sarmiento (1993) Atmospheric carbon dioxide and the ocean. *Nature* **365**, 119–25.

Sigman, D. M. and E. A. Boyle (2000) Glacial/interglacial variations in atmospheric carbon dioxide. *Nature* **407**, 859–69.

Takahashi, T. *et al.* (2002) Global sea-air CO_2 flux based on climatological surface ocean pCO_2, and seasonal biological and temperature effects. *Deep-Sea Res. II*, **49**, 1601–22.

Toggweiler, J. R. (1999) Variations of atmospheric CO_2 by ventilation of the ocean's deepest water. *Paleoceanography* **14**(5), 571–88.

Volk, T. and M. I. Hoffert (1985) Ocean carbon pumps: analysis of relative strengths and efficiencies in ocean-driven atmospheric CO_2. In *The Carbon Cycle and Atmospheric CO_2: Natural Variations Archean to Present*, Geophysical Monograph Series, vol. 32 (ed. E. T. Sundquist and W. S. Broecker), pp. 99–110. Washington, DC: AGU.